β decay in odd-A and even-even proton-rich Kr isotopes

P. Sarriguren, E. Moya de Guerra, and A. Escuderos
Instituto de Estructura de la Materia, Consejo Superior de Investigaciones Científicas, Serrano 123, E-28006 Madrid, Spain
(Received 3 April 2001; published 13 November 2001)

β-decay properties of proton-rich odd-A and even-even krypton isotopes are studied in the framework of a deformed self-consistent Hartree-Fock calculation with density-dependent Skyrme forces, including pairing correlations between like nucleons in BCS approximation. Residual spin-isospin interactions are consistently included in the particle-hole and particle-particle channels and treated in the quasiparticle random phase approximation. The similarities and differences in the treatment of even-even and odd-A nuclei are stressed. Comparison to available experimental information is shown for Gamow-Teller strength distributions, summed strengths, and half-lives. The dependence of these observables on deformation is particularly emphasized in a search for signatures of the shape of the parent nucleus.

DOI: 10.1103/PhysRevC.64.064306 PACS number(s): 23.40.Hc, 21.60.Jz, 27.50.+e

I. INTRODUCTION

One of the most exciting challenges in current nuclear physics is the understanding of nuclear systems under extreme conditions [1]. The opportunities offered by recent experimental work using beams of exotic nuclei and the corresponding theoretical efforts to describe them are of great interest, especially for nuclear structure physics and nuclear astrophysics [2].

The decay properties and cross sections for nuclear reactions of radioactive nuclei are fundamental to understand various phases in the stellar evolution, including the energy generation, the nucleosynthesis, and the abundance of elements. Since this information cannot be determined experimentally for the extreme conditions of temperature and density that hold in the interior of the star, reliable theoretical calculations for these processes are mandatory. In particular, the decay properties of proton-rich nuclei are fundamental to understand the rp process (rapid proton capture nucleosynthesis), characterized by very large proton capture reaction rates on proton rich nuclei [3]. Of special importance in this context are the waiting points like ^{72}Kr, where the rp process is inhibited and the reaction flow has to wait for the relatively slow β decay to continue. The total half-lives of the waiting points determine the speed of nucleosynthesis towards heavier nuclei as well as the isotopic abundances.

Decay properties and nuclear structure are intimately related. It is clear that a precise and reliable description of the ground state of the parent nucleus and of the states populated in the daughter nucleus is necessary to obtain a good description of the decay and, vice versa, failures to describe the decay properties would indicate that an improvement of the theoretical formalism is needed.

From a theoretical point of view the physics of exotic nuclei, characterized by very unusual ratios of neutrons and protons, can be considered as a test for the already well-established models of nuclear structure that are used to describe stable systems. Since the parameters and interactions used in the usual shell-model or mean-field calculations are determined in order to reproduce the properties of known nuclei, they may not always be appropriate for use in the calculations of nuclei approaching the drip lines.

Different microscopic models to describe the β strength are present in the literature. Models based on spherical single-particle wave functions and energies with pairing and residual interactions treated in quasiparticle random phase approximation (QRPA) were first studied in Ref. [4]. Deformation was included in Ref. [5], where a Nilsson potential was used to generate single-particle orbitals. Extensions including Woods-Saxon-type potentials [6], residual interactions in the particle-particle channel [7], Hartree-Fock (HF) mean field with separable residual interactions treated in Tamm-Dancoff approximation [8], and self-consistent approaches in spherical neutron-rich nuclei [9] and based on an energy-density functional [10] can be also found in the literature.

In a previous work [11–13] we studied ground-state and β-decay properties of even-even exotic nuclei on the basis of a deformed self-consistent HF+BCS+QRPA calculation with density-dependent effective interactions of Skyrme type. This is a well-founded approach that has been very successful in the description of spherical and deformed nuclei within the valley of stability [14]. In this method once the parameters of the effective Skyrme interaction are determined, basically by fits to global properties in spherical nuclei over the nuclear chart, and the gap parameters of the usual pairing force and the coupling strength of the residual neutron-proton pairing force are specified, there are no free parameters left. Both the residual interaction and the mean field are consistently obtained from the same two-body force. This is therefore a reliable method, suitable for extrapolations to the unstable regions approaching the drip lines. It is worth investigating whether these powerful tools designed to account for the properties of stable nuclei are still valid when approaching the drip lines.

One possible way to establish the validity of the known approaches as well as the limits of their applicability is a systematic investigation of nuclei covering the whole range from stability towards the drip lines. Exploration of series of isotopes moving away from the region of stability would fulfill these requirements, allowing us to learn how the adequacy of the description evolves in progressively more unstable nuclei.

Following the same criteria as in our previous work [11–13], we apply this formalism to the study of proton-rich krypton isotopes, including even-even as well as odd-A isotopes for the first time. The reasons why this is a region of special interest to study β decay have already been stressed in Refs. [11–13]. They include the large Q values in proton-rich nuclei [15], the competition of nuclear shapes [8,16] that characterizes this mass region, and the possibility to approach systematically the $N=Z$ isotope. Thus, we can test the validity of our formalism and look for discrepancies when approaching the drip lines.

The paper is organized as follows. We first summarize in Sec. II the method of calculation. The mean field and QRPA with residual spin-isospin interactions are introduced and explained separately for both even-even and odd-A nuclei. Gamow-Teller (GT) strengths, excitation energies, Q_{EC} values, and half-lives are also discussed. In Sec. III we present our results. We discuss similarities and differences in even-even and odd-A nuclei and analyze in detail the β-decay observables in Kr isotopes, comparing them with the available experimental data. Section IV contains the conclusions and some final remarks.

II. THEORETICAL FORMALISM

In this section we summarize briefly the theory involved in the microscopic calculations. More details can be found in Refs. [11–13]. Our method consists in a self-consistent formalism based on a deformed Hartree-Fock mean field obtained with a Skyrme interaction, including pairing correlations in the BCS approximation. We consider in this paper the force SG2 [17] of Van Giai and Sagawa, which has been successfully tested against spin and isospin excitations in spherical [17] and deformed nuclei [18]. Comparison to calculations obtained with other Skyrme forces have been made in Refs. [11,12], showing that the results do not differ in a significant way. The single-particle energies, wave functions, and occupation probabilities are generated from this mean field.

For the solution of the HF equations we follow the McMaster procedure that is based in the formalism developed in Ref. [19] and described in Ref. [20]. Time reversal and axial symmetry are assumed. The single-particle wave functions are expanded in terms of the eigenstates of an axially symmetric harmonic oscillator in cylindrical coordinates. We use 11 major shells. The method also includes pairing between like nucleons in the BCS approximation with fixed gap parameters for protons Δ_π and neutrons Δ_ν, which are determined phenomenologically from the odd-even mass differences through a symmetric five-term formula involving the experimental binding energies [21]. The values used in this work are the same as those given in Ref. [12].

For odd-A nuclei, the fields corresponding to the different interactions were obtained by doing one iteration from the corresponding self-consistent field of the closest even-even nucleus, selecting the orbital occupied by the odd nucleon according to the experimental spin and parity. For those cases where this experimental assignment is not well established we choose the orbital closer to the Fermi level. The chosen state is blocked from the BCS calculation, and we assign to it a pair occupation probability of 0.5. The effect of doing several more iterations from the even-even case, in order to see how the extra particle polarizes the core, was studied in Ref. [22] without observing significant changes. We repeated these calculations here looking for some effect on the GT strength distributions, but again the changes were negligible. According to this procedure our spin and parity assignments are as follows: $5/2^+$ for ^{77}Kr and ^{75}Kr (as determined experimentally [21]), $3/2^-$ for ^{73}Kr from the most recent experimental determination [23]. For ^{69}Kr and ^{71}Kr we take the spin and parity according to our calculations and assign $K^\pi=1/2^-$ in the first case and $K^\pi=9/2^+$ or $K^\pi=3/2^-$ in ^{71}Kr depending on the oblate or prolate shape. We describe the even-Z odd-N parent nucleus by removing one neutron from the self-consistent field of the even-even nucleus and the odd-Z even-N daughter nucleus by removing one proton. This is a proper way to describe both the parent and daughter nuclei from the same mean field. Taking (Z,N) as the even-even nucleus for reference, the parent odd-A nucleus is $(Z,N-1)$ and it decays into the daughter nucleus $(Z-1,N)$. As an example, to describe the β^+ decay of the odd-neutron parent nucleus ^{73}Kr $(Z=36,N=37)$ into the odd-proton daughter nucleus ^{73}Br $(Z=35,N=38)$, we use the mean field of the even-even nucleus ^{74}Kr $(Z=36,N=38)$.

In a previous work [12] we analyzed the energy surfaces as a function of deformation for all the even-even isotopes under study here. For that purpose, we performed constrained HF calculations with a quadrupole constraint [24] and we minimized the HF energy under the constraint of keeping fixed the nuclear deformation. Calculations in this paper are performed for the equilibrium shapes of each nucleus obtained in that way, that is, for the solutions, in general deformed, for which we obtained minima in the energy surfaces. Most of these nuclei present oblate and prolate equilibrium shapes [12] that are very close in energy. As we have mentioned, single-particle energies, wave functions, and occupation probabilities in the odd nuclei, are obtained from the converged mean fields of the even-even neighbor. Therefore, calculations in the odd nuclei are done at the corresponding equilibrium shapes of the even-even generator.

In this work, besides the odd-nuclei, we also consider a new even-even isotope, ^{70}Kr, which was not previously included in the isotope chain studied in Refs. [12,13]. We then show first in Fig. 1 the total energy of ^{70}Kr as a function of the mass quadrupole moment Q_0. The results correspond to a constrained HF+BCS calculation with the Skyrme forces SG2 and Sk3. As one can see, we obtain two minima in the energy profile: one is oblate and the other is prolate at about the same value of the quadrupole moment. These two minima are separated by about 1 MeV, the oblate being the deepest one with the two forces. Thus, ^{70}Kr follows nicely the trend observed for ^{72,74,76,78}Kr isotopes in Ref. [12], with an oblate shape favored in a shape coexistent isotope.

A. Residual interactions

To describe Gamow-Teller transitions we add to the mean field a spin-isospin residual interaction, which is expected to

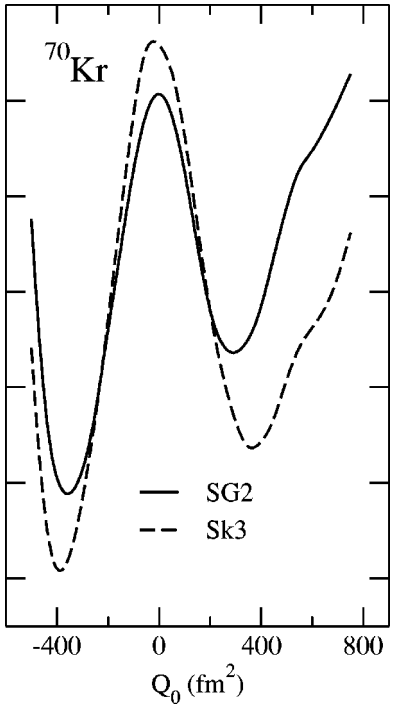

FIG. 1. Total energy of ^{70}Kr as a function of the mass quadrupole moment Q_0 obtained from a constraint HF+BCS calculation with the Skyrme forces SG2 (solid line) and Sk3 (dashed line). The distance between ticks in the vertical axis corresponds to 1 MeV but the origin is different for the two forces.

be the most relevant interaction for that purpose. This interaction contains two parts: particle-hole (ph) and particle-particle (pp). The ph part is responsible for the position and structure of the GT resonance [7,12] and is derived self-consistently from the same energy-density functional (and Skyrme interaction) as the HF equation, in terms of the second derivatives of the energy-density functional with respect to the one-body densities [25]. The ph residual interaction is finally written in a separable form by averaging the Landau-Migdal resulting force over the nuclear volume, as explained in Refs. [11,12]. The coupling strength χ_{GT}^{ph} is completely determined by the Skyrme parameters, the nuclear radius, and the Fermi momentum.

The particle-particle part is a neutron-proton pairing force in the $J^\pi=1^+$ coupling channel. We introduce this interaction in the usual way [7,13,26,27], that is, in terms of a separable force with a coupling constant κ_{GT}^{pp}, which is fitted to the phenomenology. Since the peak of the GT resonance is almost insensitive to the pp force, κ_{GT}^{pp} is usually adjusted to reproduce the half-lives [7]. However, one should be careful with the choice of this coupling constant. Since the pp force is introduced independently of the mean field, if κ_{GT}^{pp} is strong enough, it may happen that the QRPA collapses, because the condition that the ground state be stable against the corresponding mode is not fulfilled. This happens because the pp force, being an attractive force, causes the GT strength to be pushed down to lower energies with increasing values of κ_{GT}^{pp}. A careful search of the optimal strength can certainly be done for each particular case, but this is not our purpose in this work. Instead, we have chosen the same coupling constant ($\kappa_{GT}^{pp}=0.07$ MeV) for all nuclei considered here. This value was obtained [13] under the requirements of improving in general the agreement with experimental half-lives of even-even isotopes in this mass region while being still far from the values leading to the collapse.

B. Even-even nuclei

The proton-neutron QRPA phonon operator for GT excitations in even-even nuclei is written as

$$\Gamma_{\omega_K}^{+}=\sum_{\pi\nu}\left[X_{\pi\nu}^{\omega_K}\alpha_\nu^\dagger\alpha_{\bar{\pi}}^\dagger-Y_{\pi\nu}^{\omega_K}\alpha_{\bar{\nu}}\alpha_\pi\right], \tag{1}$$

where $\alpha^+(\alpha)$ are quasiparticle creation (annihilation) operators, ω_K are the excitation energies, and $X_{\pi\nu}^{\omega_K}, Y_{\pi\nu}^{\omega_K}$ the forward and backward amplitudes, respectively. From the QRPA equations the forward and backward amplitudes are obtained as [27]

$$X_{\pi\nu}^{\omega_K}=\frac{1}{\omega_K-\epsilon_{\pi\nu}}\left[2\chi_{GT}^{ph}(q_{\pi\nu}M_-^{\omega_K}+\tilde{q}_{\pi\nu}M_+^{\omega_K})-2\kappa_{GT}^{pp}(q_{\pi\nu}^U M_{--}^{\omega_K}+q_{\pi\nu}^V M_{++}^{\omega_K})\right], \tag{2}$$

$$Y_{\pi\nu}^{\omega_K}=\frac{-1}{\omega_K+\epsilon_{\pi\nu}}\left[2\chi_{GT}^{ph}(q_{\pi\nu}M_+^{\omega_K}+\tilde{q}_{\pi\nu}M_-^{\omega_K})+2\kappa_{GT}^{pp}(q_{\pi\nu}^U M_{++}^{\omega_K}+q_{\pi\nu}^V M_{--}^{\omega_K})\right], \tag{3}$$

with $\epsilon_{\pi\nu}=E_\nu+E_\pi$ the two-quasiparticle excitation energies in terms of the quasiparticle (qp) energies E_i. Here M^{ω_K} are given by

$$M_-^{\omega_K}=\sum_{\pi\nu}\left(q_{\pi\nu}X_{\pi\nu}^{\omega_K}+\tilde{q}_{\pi\nu}Y_{\pi\nu}^{\omega_K}\right), \tag{4}$$

$$M_+^{\omega_K}=\sum_{\pi\nu}\left(\tilde{q}_{\pi\nu}X_{\pi\nu}^{\omega_K}+q_{\pi\nu}Y_{\pi\nu}^{\omega_K}\right), \tag{5}$$

$$M_{--}^{\omega_K}=\sum_{\pi\nu}\left(q_{\pi\nu}^U X_{\pi\nu}^{\omega_K}-q_{\pi\nu}^V Y_{\pi\nu}^{\omega_K}\right), \tag{6}$$

$$M_{++}^{\omega_K}=\sum_{\pi\nu}\left(q_{\pi\nu}^V X_{\pi\nu}^{\omega_K}-q_{\pi\nu}^U Y_{\pi\nu}^{\omega_K}\right), \tag{7}$$

with

$$\tilde{q}_{\pi\nu}=u_\nu v_\pi\Sigma_K^{\nu\pi},\quad q_{\pi\nu}=v_\nu u_\pi\Sigma_K^{\nu\pi},\quad q_{\pi\nu}^V=v_\nu v_\pi\Sigma_K^{\nu\pi},\quad q_{\pi\nu}^U=u_\nu u_\pi\Sigma_K^{\nu\pi}, \tag{8}$$

where v's are occupation amplitudes ($u^2=1-v^2$) and $\Sigma_K^{\nu\pi}$ spin matrix elements connecting neutron and proton states with spin operators

$$\Sigma_K^{\nu\pi}=\langle\nu|\sigma_K|\pi\rangle. \tag{9}$$

Explicit expressions for these matrix elements in the cylindrical harmonic oscillator basis can be found in Ref. [11]. Note that the expressions for the X and Y amplitudes (2),(3) defined here differ from those in Refs. [11,12] by the contributions due to pp residual interactions that were not include there.

The solutions of the QRPA equations are obtained by solving first a dispersion relation, which is of fourth order in the excitation energies ω. Then, for each value of the energy the amplitudes M are determined by using the normalization condition of the phonon amplitudes. The technical procedure to solve these QRPA equations is described in detail in Ref. [27].

For even-even nuclei the GT transition amplitudes in the intrinsic frame connecting the QRPA ground state $|0\rangle(\Gamma_{\omega_K}|0\rangle=0)$ to one-phonon states $|\omega_K\rangle$ $(\Gamma^+_{\omega_K}|0\rangle=|\omega_K\rangle)$ are given by

$$\langle\omega_K|\beta^{\pm}_K|0\rangle=\mp M^{\omega_K}_{\pm}. \tag{10}$$

The Ikeda sum rule is always fulfilled in our calculations.

C. Odd-*A* nuclei

The QRPA treatment described in the above subsection is formulated for the excitations of the ground state of an even-even nucleus. The GT transition amplitudes connecting the ground state of an even-even nucleus (0qp state) to all one-phonon states in the odd-odd daughter nucleus (2qp states) are given in the intrinsic frame by Eq. (10). When the parent nucleus has an odd nucleon, the ground state can be expressed as a 1qp state in which the odd nucleon occupies the single-particle orbit of lowest energy. Then two types of transitions are possible, which are represented schematically in Fig. 2.

(i) The first type of transitions are phonon excitations in which the odd nucleon acts only as a spectator. We call them three-quasiparticle transitions. In the intrinsic frame, the transition amplitudes in this case are basically the same as in the even-even case but with the blocked spectator excluded from the calculation,

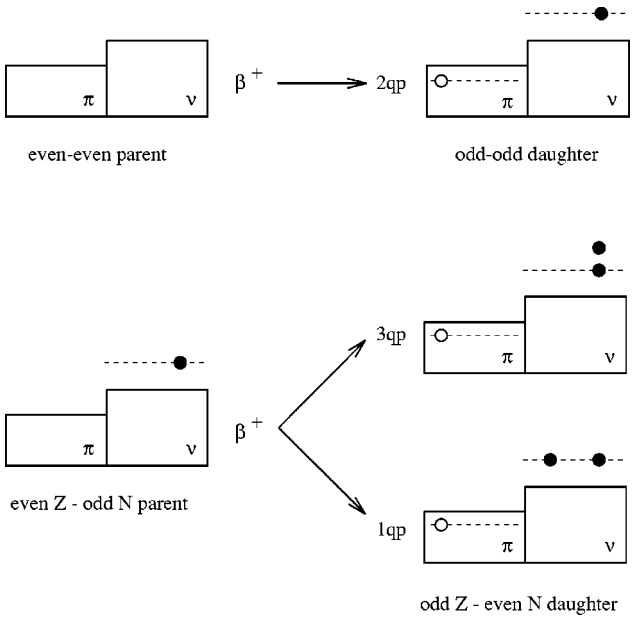

FIG. 2. Schematic picture to illustrate the different types of β^+ decay in the extreme single-particle model. In the case of an even-even parent we have 2qp transitions. In the case of an odd neutron parent there are two types of transitions. In the 3qp case the unpaired neutron in the parent nucleus acts as an spectator. The 1qp type of transitions are those involving the unpaired neutron.

$$\langle f|\beta^{\pm}_K|i\rangle_{3qp}=\langle\omega_K,1qp|\beta^{\pm}_K|0,1qp\rangle=\mp M^{\omega_K}_{\pm}. \tag{11}$$

(ii) The other type of transitions are those involving the odd nucleon. We call them one-quasiparticle transitions. We introduce as usual [5,6,27] phonon correlations to the quasiparticle transitions in first-order perturbation, taking into account the part of the GT interaction that contains terms linear in the $\eta_{\nu\pi}=\alpha^{\dagger}_{\nu}\alpha_{\pi}$ operator. The transition amplitudes for the correlated states can be found in Ref. [27]. Here, we give the explicit expression for the transition amplitude corresponding to the Kr isotopes, that is, a β^+ decay of an odd-neutron parent nucleus decaying into an odd-proton daughter nucleus:

$$\begin{aligned}\langle f|\beta^+_K|i\rangle_{1qp}&=\langle\pi_{corr}|\beta^+_K|\nu_{corr}\rangle\\
&=q^V_{\pi\nu}+2\chi^{ph}_{GT}\Big\{q^V_{\pi\nu}\sum_{\omega_K}[(M^{\omega_K}_+)^2E_{\pi}(\nu,\omega_K)+(M^{\omega_K}_-)^2E_{\nu}(\pi,\omega_K)]-q^U_{\pi\nu}\sum_{\omega_K}M^{\omega_K}_+M^{\omega_K}_-[E_{\pi}(\nu,\omega_K)+E_{\nu}(\pi,\omega_K)]\Big\}\\
&+2\kappa^{pp}_{GT}\Big\{\tilde{q}_{\pi\nu}\sum_{\omega_K}[M^{\omega_K}_+M^{\omega_K}_{++}E_{\pi}(\nu,\omega_K)-M^{\omega_K}_-M^{\omega_K}_{--}E_{\nu}(\pi,\omega_K)]-q_{\pi\nu}\sum_{\omega_K}[M^{\omega_K}_+M^{\omega_K}_{--}E_{\pi}(\nu,\omega_K)\\
&-M^{\omega_K}_-M^{\omega_K}_{++}E_{\nu}(\pi,\omega_K)]\Big\},\end{aligned} \tag{12}$$

where q's and M's are given in Eqs. (4)–(8). In this expression, $E_{\pi}(\nu,\omega_K)$ is in principle given by $E_{\pi}(\nu,\omega_K)=1/(E_{\pi}-E_{\nu}-\omega_K)$ and a similar expression for $E_{\nu}(\pi,\omega_K)$ changing ν into π. Nevertheless, in order to avoid accidental singularities, we introduce a width $d=0.5$ MeV in the same way as it was done for the first time in Ref. [6]:

$$E_\pi(\nu,\omega_K)=\frac{E_\pi-E_\nu-\omega_K}{(E_\pi-E_\nu-\omega_K)^2+d^2}. \tag{13}$$

For simplicity we speak of 1qp, 2qp, and 3qp states, but it should be clear that we always mean QRPA-correlated states.

Once the intrinsic amplitudes $\langle f|\beta_K^\pm|i\rangle$ are calculated in Eqs. (11),(12), the Gamow-Teller strength B_{GT} for a transition $I_i\rightarrow I_f$ can be obtained as

$$\begin{aligned}B_{GT}^\pm&=\sum_{M_i,M_f,\mu}|\langle I_fM_f|\beta_\mu^\pm|I_iM_i\rangle|^2=\left\{\sum_\rho\left[\langle I_iK_i1\rho|I_fK_f\rangle\langle\phi_{K_f}|\beta_\rho^\pm|\phi_{K_i}\rangle+(-1)^{I_i-K_i}\langle I_i-K_i1\rho|I_fK_f\rangle\langle\phi_{K_f}|\beta_\rho^\pm|\phi_{\bar{K}_i}\rangle\right]\right\}^2\\&=\delta_{K_i,K_f}[\langle I_iK_i10|I_fK_f\rangle\langle\phi_{K_f}|\beta_0^\pm|\phi_{K_i}\rangle+\delta_{K_i,1/2}(-1)^{I_i-K_i}\langle I_i-K_i11|I_fK_f\rangle\langle\phi_{K_f}|\beta_{+1}^\pm|\phi_{\bar{K}_i}\rangle]^2\\&\quad+\delta_{K_f,K_i+1}\langle I_iK_i11|I_fK_f\rangle^2\langle\phi_{K_f}|\beta_{+1}^\pm|\phi_{K_i}\rangle^2+\delta_{K_f,K_i-1}\langle I_iK_i1-1|I_fK_f\rangle^2\langle\phi_{K_f}|\beta_{-1}^\pm|\phi_{K_i}\rangle^2,\end{aligned} \tag{14}$$

in units of $g_A^2/4\pi$. To obtain this expression we have used the initial and final states in the laboratory frame expressed in terms of the intrinsic states $|\phi_K\rangle$ using the Bohr-Mottelson factorization [28].

Equation (14) can be particularized for even-even parent nuclei. In this case $I_i=K_i=0$, $I_f=1$, and $K_f=0,1$.

$$B_{GT}^\pm=\frac{g_A^2}{4\pi}\{\delta_{K_f,0}\langle\phi_{K_f}|\beta_0^\pm|\phi_0\rangle^2+2\,\delta_{K_f,1}\langle\phi_{K_f}|\beta_1^\pm|\phi_0\rangle^2\}. \tag{15}$$

D. Excitation energies, Q_{EC} values, and half-lives

Concerning the excitation energy of the daughter nuclei to which we refer all the GT strength distributions in this paper, we have to distinguish again between the case of even-even and odd-A parents. In the case of even-even systems, this excitation energy is simply given by

$$E_{\mathrm{ex}[(Z,N)\rightarrow(Z-1,N+1)]}=\omega-E_{\pi_0}-E_{\nu_0}, \tag{16}$$

where E_{π_0} and E_{ν_0} are the lowest quasiparticle energies for protons and neutrons, respectively.

In the case of an odd-A nucleus we have to deal with 1qp and 3qp transitions. Let us consider here our case of an odd-neutron parent decaying by β^+ into an odd-proton daughter. For 1qp transitions, since the unpaired neutron state is the only neutron state involved in the transition, the excitation energy is

$$E_{\mathrm{ex,1qp}(Z,N-1)\rightarrow(Z-1,N)}=E_\pi-E_{\pi_0}. \tag{17}$$

On the other hand, in the 3qp case where the unpaired neutron acts as a spectator, the excitation energy with respect to the ground state of the daughter nucleus is

$$E_{\mathrm{ex,3qp}\,(Z,N-1)\rightarrow(Z-1,N)}=\omega+E_{\nu,\mathrm{spect}}-E_{\pi_0}. \tag{18}$$

This implies that the lowest excitation energy of 3qp type is of the order of twice the neutron pairing gap. In the Kr isotopes under study here, $\Delta\sim1.5$–2 MeV [12]. Therefore, all the strength contained in the low-excitation-energy region, below typically 3–4 MeV in the odd-A nuclei studied in this paper, must correspond to 1qp transitions. Thus, the low excitation energy region (below twice the neutron pairing gap) in a β^+ decay from an odd-neutron nucleus, basically tells us about the proton spectrum.

We should also mention that in odd-A nuclei we have considered the transitions to the rotational states as well. We consider only those states built on the K_f bandheads, which are not forbidden by the selection rules of the Gamow-Teller operator in the allowed approximation. This means that we calculate according to Eq. (14) the GT strength corresponding to transitions from an initial $I_i=K_i$ state to final states characterized by (i) $I_f=K_f$ when $K_f=K_i+1$, (ii) $I_f=K_f$ and $I_f=K_f+1$ when $K_f=K_i$, and (iii) $I_f=K_f$, $I_f=K_F+1$, and $I_f=K_f+2$ when $K_f=K_i-1$.

Accordingly, we have added to the excitation energies ω_K a standard Bohr-Mottelson rotational energy [28]. The purpose of the inclusion in our calculation of the transitions to the rotational states is to take into account in a more reliable way the fragmentation of the GT strength and the density of excitation energies. Thus, in our calculations we estimate the moment of inertia by using a mean value between the two extreme macroscopic models, rigid rotor (rr) and irrotational flow (if) model, whose predictions are usually upper and lower boundary values of the experimental moments of inertia.

Q_{EC} values are also determined differently depending on the even or odd number of nucleons. The Q_{EC} value is given by $Q_{EC}=[M_{\mathrm{parent}}-M_{\mathrm{daughter}}+m_e]c^2$, where M's are the nuclear masses (binding energies of the electrons have been neglected). For the β^+ decay of an odd-neutron parent we have

$$\begin{aligned}Q_{EC,(Z,N-1)\rightarrow(Z-1,N)}&=m_\pi-m_\nu+m_e+\lambda_{\pi(Z-2,N-2)}\\&\quad-\lambda_{\nu(Z-2,N-2)}-E_{\pi(Z-2,N-2)}\\&\quad+E_{\nu(Z-2,N-2)},\end{aligned} \tag{19}$$

where λ is the Fermi level and E is the lowest quasiparticle energy $E=\sqrt{(\epsilon-\lambda)^2+\Delta^2}$. The Q value for β^+ decay is simply $Q_{\beta^+}=Q_{EC}-2m_e$.

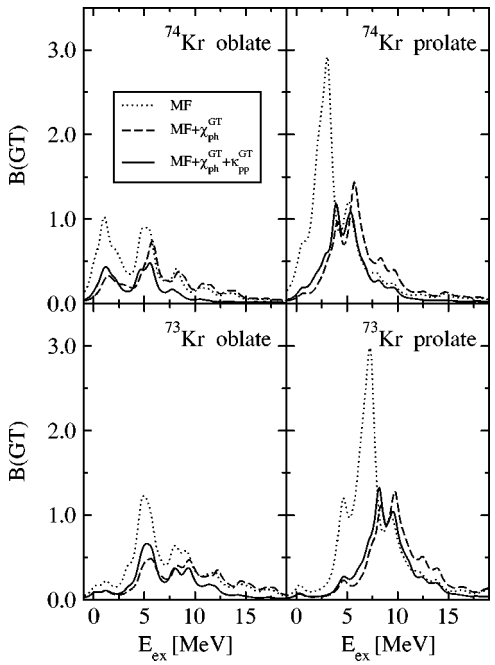

FIG. 3. Gamow-Teller strength distributions $[g_A^2/4\pi]$ in ^{73,74}Kr isotopes plotted versus the excitation energy of the corresponding daughter nucleus ^{73,74}Br, respectively. The calculations are performed in HF+BCS approximation (dotted lines denoted by MF) and in QRPA including only the ph residual interaction (dashed line) and including both ph and pp residual interactions (solid line).

These expressions can be compared to that corresponding to an even-even nucleus (Z,N):

$$Q_{EC,(Z,N)\to(Z-1,N+1)} = m_\pi - m_\nu + m_e + \lambda_{\pi,(Z-2,N)} - \lambda_{\nu,(Z,N)} - E_{\pi,(Z-2,N)} - E_{\nu,(Z,N)}. \quad (20)$$

The half-lives for the β^+/EC decay are obtained using the standard definition (see for instance Ref. [12]), involving sums over all possible final states within the Q window reached in the decay and including standard quenching factors [29].

The Fermi integrals required for computation of half-lives have been obtained numerically for each value of the charge of the daughter nucleus Z and the maximum energy available W_0 in β decay, as explained in Ref. [30].

III. RESULTS

In this section we present and discuss the results obtained for the GT strength distributions, half-lives, and summed strengths in the proton-rich Kr isotopes. The results correspond to QRPA calculations with the Skyrme force SG2 and they have been performed for the nuclear shapes that minimize the HF energy. Before discussing the figures we note that the GT strength distributions are plotted versus the excitation energy of the daughter nucleus. The distributions of the GT strength in Figs. 3, 5, and 6 have been folded with $\Gamma=1$ MeV width Gaussians to facilitate the comparison among the various calculations, so that the original discrete spectrum is transformed into a continuous profile. The distributions in those figures are given in units of $g_A^2/4\pi$ and one should keep in mind that a quenching of the strength is expected on the basis of the observed quenching in charge exchange reactions and spin $M1$ transitions in stable nuclei, where $g_{s,\mathrm{eff}}$ is also known to be approximately $0.7g_{s,\mathrm{free}}$. Therefore, a reduction factor of about 2 is expected in these strength distributions in order to compare with experiment. This factor is of course taken into account when comparison to experimental half-lives, summed strengths, and GT strengths is made.

A. Effect of the residual interaction

We can see in Fig. 3 the effect of the residual interaction treated in the QRPA on the uncorrelated calculation (dotted lines denoted by MF). We do that on the example of ^{73,74}Kr for the oblate and prolate shapes that minimize the energy obtained with the Skyrme force SG2. The coupling strengths of the ph and pp residual interactions are $\chi_{GT}^{ph}=0.37$ MeV and $\kappa_{GT}^{pp}=0.07$ MeV, respectively. Both ph and pp residual interactions reduce the GT strength. The residual forces produce also a displacement of the GT strength, which is to higher energies in the case of the repulsive ph force and to lower energies in the case of the attractive pp force.

These effects are common to even-even and odd-A isotopes. Nevertheless, we observe that the effect of the residual interaction in odd-A nuclei is very small in the low-energy tail of the GT strength distribution. This is especially true for the pp force. The reason for that can be understood from the fact that the lowest-lying transitions are affected by the residual force only through the weak correlations with phonons treated in first order perturbation.

This feature has also important consequences when one considers the half-lives because they depend only on the distribution of the strength below the Q_{EC}-energy window. Therefore, the pp interaction will affect the half-lives differently if we deal with even-even or odd-A nuclei. In Fig. 4 we have plotted the half-lives of the ^{71,72,73,74}Kr isotopes as a function of the strength κ_{GT}^{pp}. As we can see from this figure the half-lives decrease with increasing values of κ_{GT}^{pp}, but in a different way depending on the isotopes. We can see that the half-lives of odd-A nuclei have a very smooth, almost flat, behavior with the pp force, while the half-lives of even-even nuclei present a stronger dependence on the pp force. Decreasing of half-lives with κ_{GT}^{pp} can be understood from the fact that the pp force is attractive and therefore tends to concentrate the strength to lower energies. The reason for the smoother decrease of half-lives in the odd-A isotopes is related to the smaller effect of the pp force in the low-energy tail of the GT strength distribution in odd-A nuclei, previously discussed.

The optimum value of κ_{GT}^{pp} to reproduce the half-life depends, among other factors, on the nucleus, shape, and Skyrme interaction and a case-by-case fitting procedure could be carried out. Since the half-lives are practically insensitive to this force in odd-A nuclei, this fit could be restricted to even-even nuclei. In Ref. [13] we considered this dependence in various even-even isotopes in the mass region

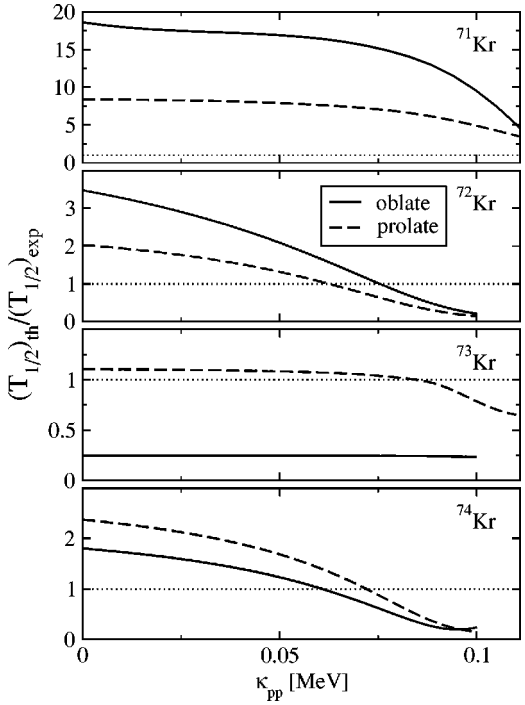

FIG. 4. Ratios of calculated to experimental half-lives in Kr isotopes as a function of the coupling strength of the pp force.

$A\sim 70$ (Ge, Se, Kr, and Sr) and arrived at the conclusion that a value of $\kappa_{GT}^{pp}=0.07$ MeV improves the agreement with experiment in most cases. Thus, we also use in this paper the same coupling strength for the pp force.

B. Comparison of even-even and odd-A GT strengths

To further illustrate the relative importance of the different types of contributions to the GT strength in odd-A nuclei, we show in Fig. 5 the GT strengths (solid) decomposed into their 1qp (dotted) and 3qp (dashed) contributions. The picture emerging from the analysis of this figure is that the GT strength distributions in odd-A nuclei can be divided into two different regions. One is the energy region below twice the pairing gap, where the individual excitations are determined by the quasiparticle proton (neutron) energies in the case of an odd-neutron (odd-proton) parent nucleus. This region is of relevance for β^+ decay since it appears within the Q window. The other region at higher energies is dominated by 3qp excitations, where the odd nucleon acts as a spectator. The strength contained here is much larger than in the low-energy region because many more configurations are possible but only in the very-proton-rich isotopes this is accessible by β^+ decay.

Figure 6 contains a summary of the results on GT strengths obtained in this work. In this figure we can see our HF+BCS+QRPA Gamow-Teller strength distributions predicted by the Skyrme force SG2 for the whole Kr isotopic chain including odd-A and even-even nuclei.

The trend observed in the GT strength distributions of both odd-A and even-even isotopes is similar. We can see that the most unstable isotopes have the largest strengths which are also placed at higher energies. As we move into the stable isotopes by increasing the number of neutrons, the GT resonance appears at lower excitation energies and contains less and less strength. Also the Q_{EC} window, represented by the vertical line, becomes smaller and smaller.

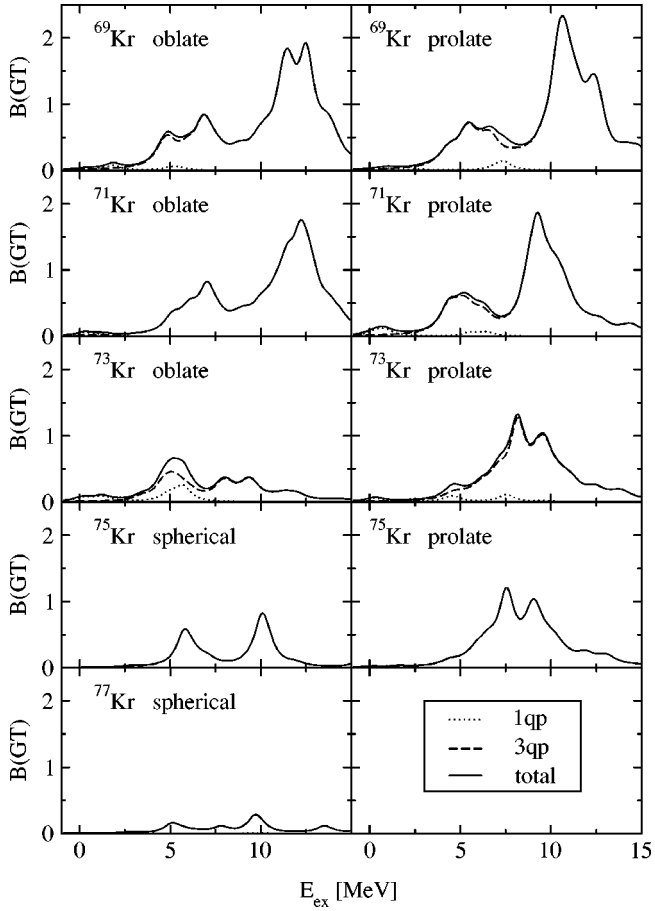

FIG. 5. Decomposition of the total GT strength distribution into their 1qp and 3qp contributions (see text).

We can observe also the similarity between the even-even and odd-A partners. If we compare the strengths for an even-even (N,Z) nucleus with that of the corresponding odd-A $(N-1,Z)$ nucleus, we can see that they are about the same once the low-energy region of about twice the neutron pairing gap (between 3 and 4 MeV depending on the case) is suppressed.

We can also observe that the different profiles of the GT strength distributions corresponding to the various shapes of a given isotope can be used in certain cases as a signature of the nuclear shape.

C. Low-energy GT strength and comparison to experiment

Now we concentrate on the energy region below Q_{EC} and discuss the possibilities to discriminate between different shapes by β^+-decay experiments. We also compare with the available experimental data. We perform this detailed analysis by plotting not the folded strengths as it was done in the previous figures, but the individual excitations as they come from the calculation. The GT strengths have been quenched

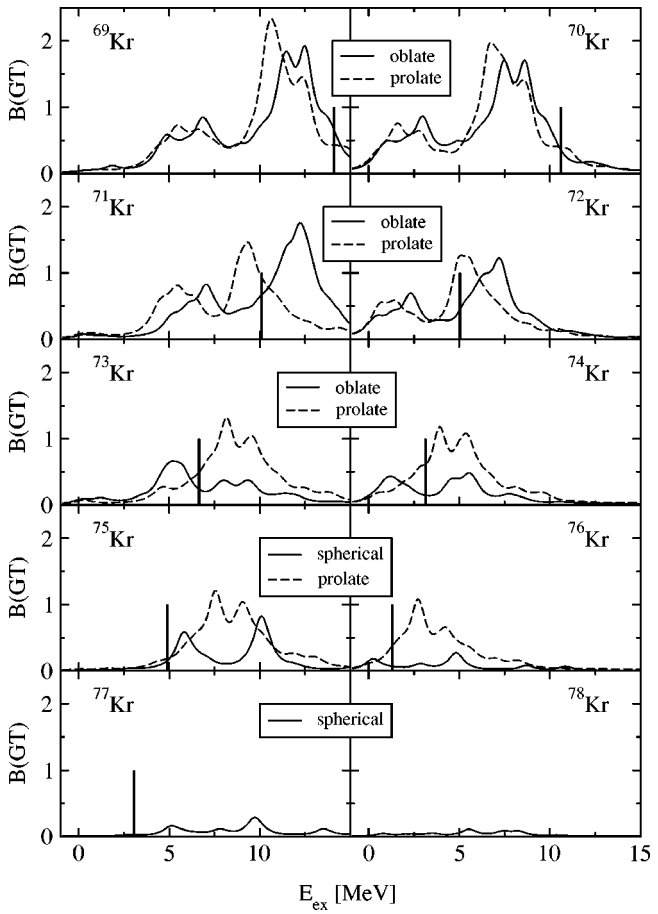

FIG. 6. Gamow-Teller strength distributions $[g_A^2/4\pi]$ as a function of the excitation energy of the daughter nucleus [MeV]. The results correspond to the Skyrme force SG2 in QRPA for the various shapes of the even-even and odd-*A* Krypton isotopes.

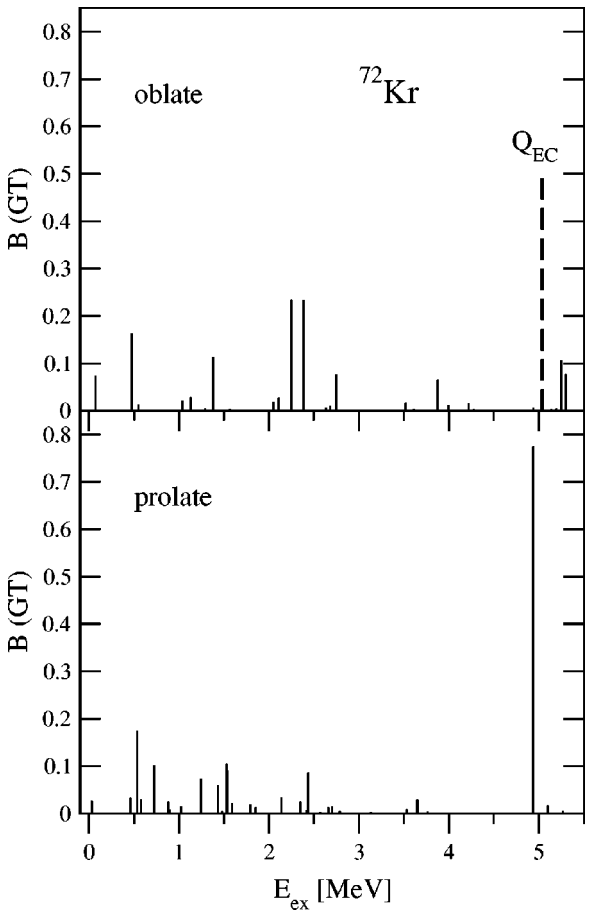

FIG. 7. Gamow-Teller strength transitions in the β^+-decay of ^{72}Kr as a function of the excitation energy of the daughter nucleus ^{72}Br.

with the same factor used to calculate the half-lives. In Figs. 7–9we can see these results for the even-even isotopes ^{72,74,76}Kr, respectively.

Figure 7 for ^{72}Kr includes the results from our QRPA calculations with the force SG2 with oblate and prolate shapes. Below an excitation energy of about 2 MeV we can see that the distribution of the GT strength predicted by the oblate or prolate shapes is qualitatively very similar although the prolate shape gives somewhat larger strength. We obtain peaks at 0.5 MeV and 1.5 MeV in both cases and they are in agreement with preliminary data on this nucleus [31]. Therefore, it will be hard to distinguish between the two shapes. On the other hand, if we look into the energy range from 2 MeV up to Q_{EC}, we can see a strong double peak that appears in the oblate case between 2 and 2.5 MeV. The strength in this region is about 3 times larger than the strength of the first peak at 0.5 MeV and it is almost absent in the prolate case. The appearance or absence of this peak at 2 MeV could be the signature of an oblate or prolate shape, respectively. It is also worth mentioning the huge peak appearing in the prolate case very close to the Q_{EC} value. If it could be seen experimentally, it would be a clear signature in favor of a prolate shape. We can see in Table I the total measured GT strength below 1.836 MeV [32] compared to our results with the two shapes, where oblate shape seems to be favored.

Figure 8 shows the results in ^{74}Kr. Experimental data are from Ref. [33]. We can distinguish two regions in this isotope. At energies below 2 MeV we find that the oblate shape predicts much more strength than the prolate shape and the opposite happens beyond 2 MeV. Therefore, measuring the GT strength distribution in ^{74}Kr up to Q_{EC} would help to discriminate between the two shapes. If the strength is concentrated below 2 MeV, it will correspond to an oblate shape, while if it is concentrated between 2 and 3 MeV, it will correspond to a prolate shape. A comparison of the strength contained below 1 MeV is made in Table I. The experimental summed strength [33] lies between the predictions of the two shapes but it is closer to the strength produced by the oblate shape.

In Fig. 9 we show the results for ^{76}Kr corresponding to the spherical and prolate shapes that minimize the energy in this nucleus. Experimental data are from Ref. [34]. In this case, an isolated single peak in the measured strength at very low excitation energy would be the signature of a spherical parent, while a peak close to the Q_{EC} limit would be the signature of a prolate parent. Comparison with the available data seems to favor the spherical shape. This is also true if we compare the total GT strengths contained below 1 MeV,

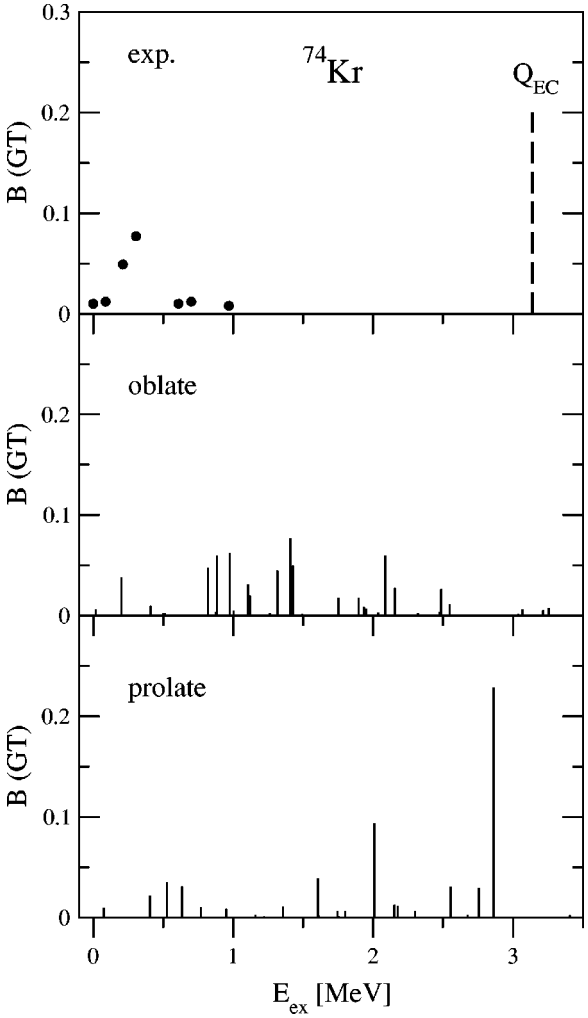

FIG. 8. Same as in Fig. 7 for the decay of ^{74}Kr. Experimental data are from [33].

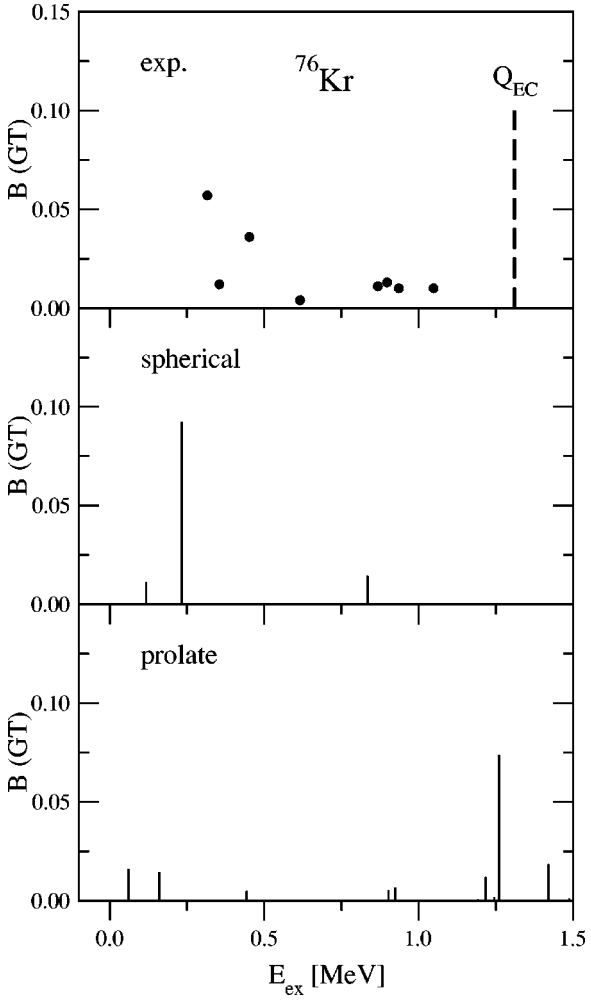

FIG. 9. Same as in Fig. 7 for the decay of ^{76}Kr. Experimental data are from [34].

as can be seen in Table I, where the strength generated by the spherical shape is much closer to experiment.

Next Figs. 10–13 correspond to the odd-A nuclei ^{73,75}Kr. In Fig. 10 we can see our results for the oblate and prolate shapes of ^{73}Kr compared to the experimental data from Ref. [23]. The first thing to mention is that the experimental data have been taken differently in the two energy ranges below and above 3.5 MeV. Below 3.5 MeV the data have been extracted from direct detection of the gamma rays. Beyond this energy they have been extracted from proton delayed detection and have big errors. A new effort to measure experimentally the entire energy range up to Q_{EC} with large efficiency gamma ray detectors is under way at ISOLDE [35]. Until these data become available and confirm the present measurements, the data measured above 3.5 MeV should be considered as partial because part of the strength escapes observation due to the high level density [31]. The summed GT strengths in the two energy regions can be seen in Table I. The experimental data appear between the predictions of the oblate and prolate shapes, the oblate one being larger.

Comparison to the data of the GT strength distributions below 3.5 MeV shows that both oblate and prolate shapes produce similar strength in the very low excitation energy range below 0.5 MeV, which is compatible with experiment. At higher energies the prolate shape does not generate strength up to 4 MeV while the oblate shape generates two bunches at 1 MeV and 3.5 MeV that compare better with experiment. Above 4 MeV, the strength increases and the prolate shapes produces two bumps at 4.5 and 6 MeV, while the oblate shape produces a wide peak from 4.5 to 6.5 MeV with a huge strength at an excitation energy of 5.5 MeV. It is also worth mentioning that the structure of the GT transitions in the theoretical calculations can be analyzed taking into account the rotational nature of the final states reached by the allowed GT transition. As we have already mentioned, since in this case we are considering the transitions $K_i^\pi = 3/2^- \rightarrow K_f^-$ with $K_f = 1/2,3/2,5/2$, when we reach a final state with $K_f^\pi = 1/2^-$, we consider the rotational states with $I_f = 1/2^-,3/2^-,5/2^-$. The strengths of these states are given by the geometrical Clebsch-Gordan factors in Eq. (14) and their excitation energies by the rotational energies. Similar arguments apply to the transitions to $K_f^\pi = 3/2^-$, where we consider the rotational states with $I_f = 3/2^-,5/2^-$. For $K_f^\pi = 5/2^-$, the only case to account for is $I_f = 5/2^-$. On this basis we can now see that the two peaks below 0.5 MeV in

TABLE I. Comparison of the GT strengths contained below some given excitation energy between experimental measurements ([32] for ^{72}Kr, [23] for ^{73}Kr, [33] for ^{74}Kr, [36] for ^{75}Kr, and [34] for ^{76}Kr), and theoretical calculations.

	Expt	Oblate	Prolate
^{72}Kr ($E_{ex} \leqslant 1.836$ MeV)	0.5 ± 0.1	0.5	0.8
^{73}Kr ($E_{ex} \leqslant 3.5$ MeV)	0.10 ± 0.02	0.19	0.06
^{73}Kr (4.0 MeV$\leqslant E_{ex} \leqslant$6.5 MeV)	0.83 ± 0.60	0.98	0.42
^{74}Kr ($E_{ex} \leqslant 1$ MeV)	0.20	0.23	0.12
^{75}Kr ($E_{ex} \leqslant 2.2$ MeV)	0.08	0.00 (sph)	0.05
^{76}Kr ($E_{ex} \leqslant 1$ MeV)	0.16	0.18 (sph)	0.05

the prolate case are the members of a rotational band $I_f = K_f = 3/2^-$ and $I_f = 5/2^-, K_f = 3/2^-$. Similarly we can identify the low-lying structure in the oblate case as the members of several rotational bands. This can be seen more easily in Fig. 11, where we have plotted the excitation energies in the daughter nucleus ^{73}Br of the states reached by β^+ decay. In this figure we have also added by dotted lines the first forbidden transitions that correspond to $\Delta J = 1$ with parity change, that is, states $1/2^+, 3/2^+, 5/2^+$. Although we have not calculated their GT strength, their excitation energies have been plotted in the figure. We can see that the agreement with experiment is very reasonable in the oblate case. We get concentrations of states at the same energies and the total number of states is similar. In this figure we can follow more easily the structure of the bands. For example, in the prolate case we can see that the lowest $3/2^-$ has a $5/2^-$ associated, the next $1/2^-$ has two states $3/2^-$ and $5/2^-$ associated and so on.

A similar analysis has been done in Figs. 12 and 13 for

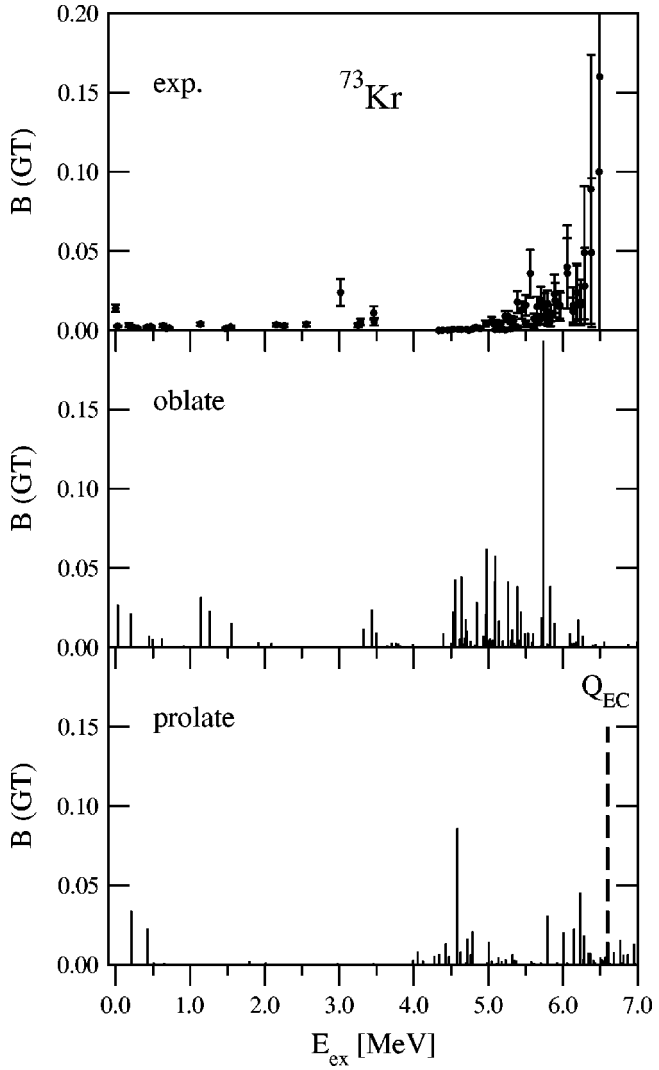

FIG. 10. Same as in Fig. 7 for the decay of ^{73}Kr. Experimental data are from [23].

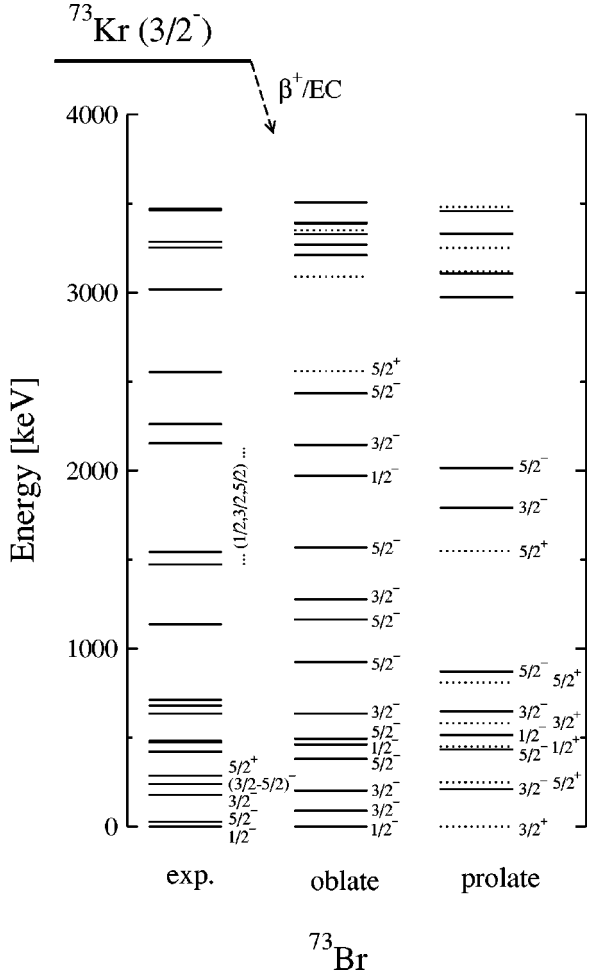

FIG. 11. Experimental and calculated decay schemes for ^{73}Kr.

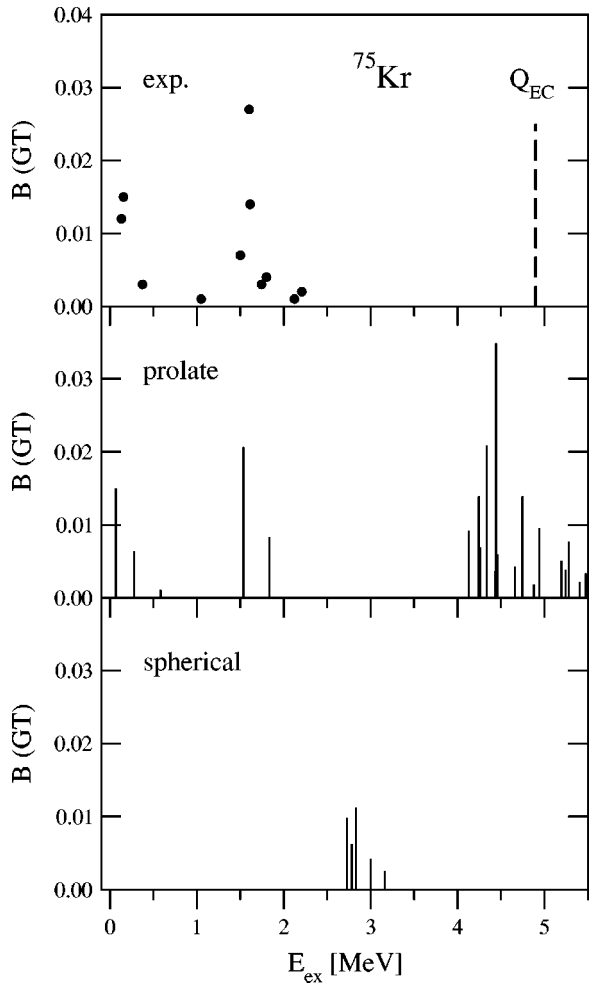

FIG. 12. Same as in Fig. 7 for the decay of ^{75}Kr. Experimental data are from [36].

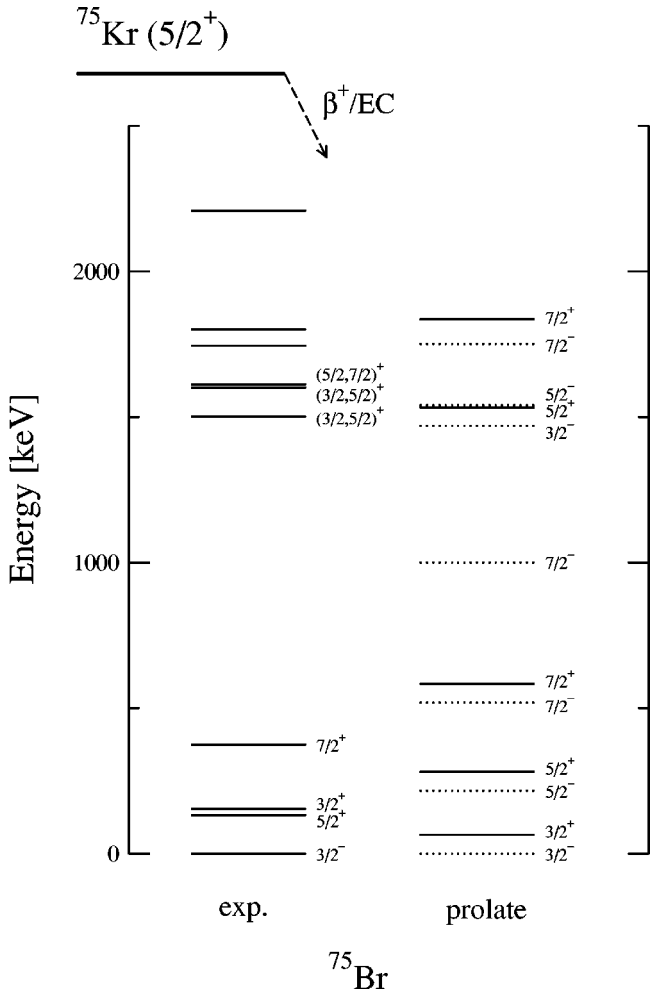

FIG. 13. Same as in Fig. 11 for the decay of ^{75}Kr.

^{75}Kr. In Fig. 12 we can see the GT strengths in the prolate and spherical cases compared to the experimental data from Ref. [36] taken up to 2.5 MeV. The summed strengths can be also compared in Table I. The spherical shape does not produce any strength in the Q_{EC} window except a small bunch of states around 3 MeV. On the other hand, the prolate shape generates strength at the right position although a little bit smaller than experiment. This shape also predicts some strength close to Q_{EC}, which is not present in the spherical case. Figure 13 shows the experimental low-lying energy spectrum compared to our calculation for the prolate shape. In our results we can identify the origin of these excitations. We have a low-lying $3/2^+$,$5/2^+$,$7/2^+$ rotational triplet and a $5/2^+$,$7/2^+$ doublet. They correspond well with the experimental energies. We should remember that the spacing in the rotational energies is determined by the moment of inertia, and we are using a rough estimate. Using a moment of inertia a little bit larger, the energy levels become compressed and agree better with the experimental spacing. We have also added by dotted lines the energies of first forbidden transitions.

Experimental information on the decay of ^{71}Kr is available for the low-lying states [37]. In that reference, final states for GT decay were reported to the ground state of ^{71}Br and to excited states at 9 and 207 keV. However, the spin-parity assignment of these states, as well as the assignment to the ground state of the parent nucleus ^{71}Kr, are still controversial [38]. We can see in Fig. 14 the results of our mean-field calculations with the force SG2 for the oblate and prolate shapes of ^{72}Kr. The vertical axis is the neutron occupation probability and the horizontal one is the neutron single-particle energy. The deformed single-particle states are labeled by K^π. We can see that the picture is compatible with several spin and parity assignments for the odd-neutron isotope ^{71}Kr. If we consider the neutron level closest to Fermi level in Fig. 14, the spin-parity assignment would be $9/2^+$ for the oblate shape and $3/2^-$ for the prolate shape. On the other hand, the assumption taken in Ref. [37] was $5/2^-$, which is also close to Fermi level. We therefore consider these two possibilities for each shape.

We show in Fig. 15 the results for the GT strengths from our calculations assuming the above mentioned possibilities for the spin and parity of the parent nucleus, $5/2^-$ as was taken in Ref. [37], as well as $9/2^+$ in the oblate case and $3/2^-$ in the prolate case. We can also see the spin and parity of each GT excitation.

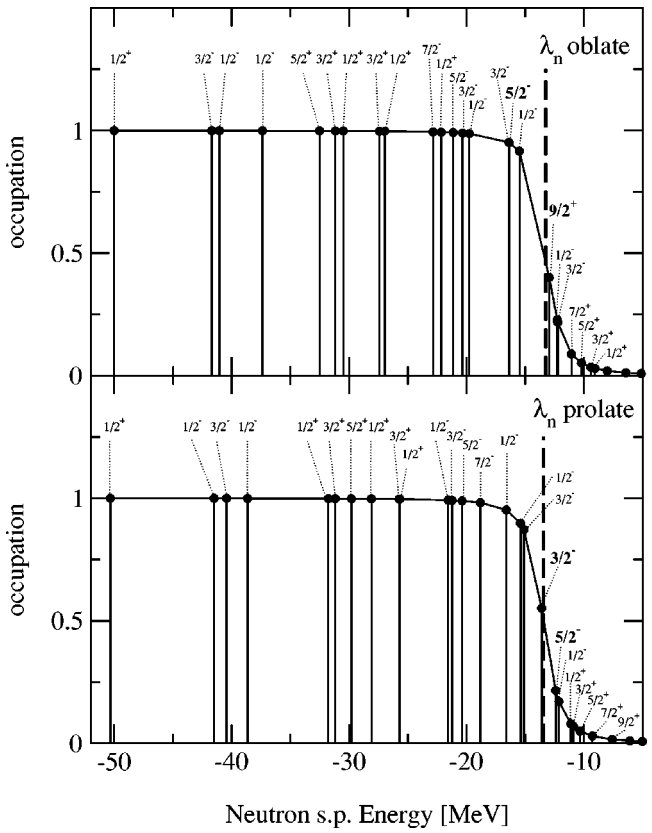

FIG. 14. Neutron single-particle energies and occupation probabilities of the intrinsic states K^{π} calculated with the force SG2 for the two shapes, oblate and prolate, which minimize the energy in ^{72}Kr. λ_n are the neutron Fermi energies.

D. Q_{EC} values and half-lives

Experimental Q_{EC} and $T_{1/2}$ values are plotted as circles in Fig. 16 for the krypton isotopes considered in this work. The data have been taken from Ref. [21], except for the isotopes ^{70,71}Kr, where we have used the more recent data from Ref. [37]. These values are compared to our theoretical results represented by the vertical lines. The extreme values of these vertical lines correspond to the results obtained from the various shapes using the forces SG2 and Sk3. This has been done in order to have a better idea of the theoretical spread of the results. The agreement is in general good for both Q_{EC} and half-lives. This is notorious because there is a very large range of variation (seven orders of magnitude) for half-lives. Q_{EC} values are well reproduced with the exception of ^{70}Kr, where we obtain a value below experiment.

We can also see that the calculations fail to account for the half-lives of the most unstable nuclei ^{70}Kr and ^{71}Kr. Nevertheless, it should be mention that the calculations correspond to GT transitions neglecting possible contributions from Fermi transitions. But Fermi transitions might play a significant role to obtain the total decay rates in nuclei where $N \sim Z$. Indeed, we have calculated the Fermi strength distributions and evaluated the corresponding half-lives. The calculation of Fermi transitions follows closely that of Gamow-Teller transitions. One should simply use an isospin-isospin residual interaction with a coupling strength derived from the Skyrme force as shown in Ref. [11] and replace the spin matrix elements between proton and neutron states given in Eq. (9) by the overlaps $\langle \nu | \pi \rangle$. Of course, only $K=0$ components will survive.

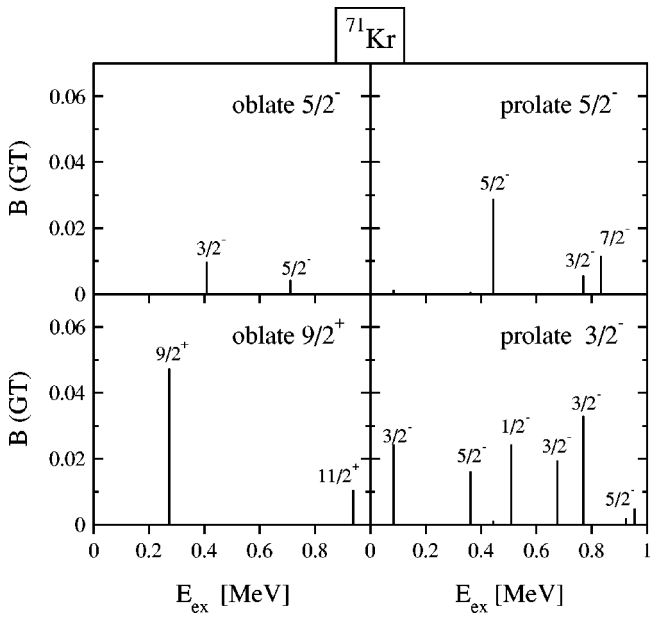

FIG. 15. Energy distribution of the Gamow-Teller strength in ^{71}Kr assuming different spins and parities of the ground state in the parent nucleus.

We find that the half-lives corresponding to Fermi transitions are negligible as compared to the GT half-lives except in the isotopes ^{70,71,72,73}Kr, where they are comparable and therefore one should not neglect their contribution. We can see in Fig. 16, the new results for the total half-lives once the contribution from Fermi transitions have been included. They are given by the vertical lines located at the right side in the half-lives of the ^{70,71,72,73}Kr isotopes. The agreement with experiment improves in the cases of ^{70,71}Kr but we are still above the experiment. Nevertheless, it should be mentioned that if we use the experimental Q_{EC} value in ^{70}Kr, instead of the Q_{EC} result from our calculations, we get agreement with the experimental half-life. Thus, the discrepancy found in the half-life of ^{70}Kr is entirely due to the discrepancy in the Q_{EC} value.

We can observe in Fig. 16 a nice trend that can be followed by the auxiliary dotted lines joining the experimental data of even-even isotopes on one hand and the odd-A on the other. The growing Q_{EC} trends in the two lines of Fig. 16 are dictated by the increase of $(\lambda_{\pi} - \lambda_{\nu})$ as one approaches the proton drip line. This behavior can be qualitatively understood in the case of Q_{EC} from their expressions given by Eqs. (19),(20). As we have mentioned earlier, the only exception to this trend appears in the experimental Q_{EC} value of ^{70}Kr, which is clearly above the theoretical value. Since in this case the daughter nucleus ^{70}Br is odd-odd $N=Z$, one may argue that the observed jump from the regular trend in Q_{EC} and $T_{1/2}$ is due to an extra neutron-proton binding, which is not taken into account in the present calculation.

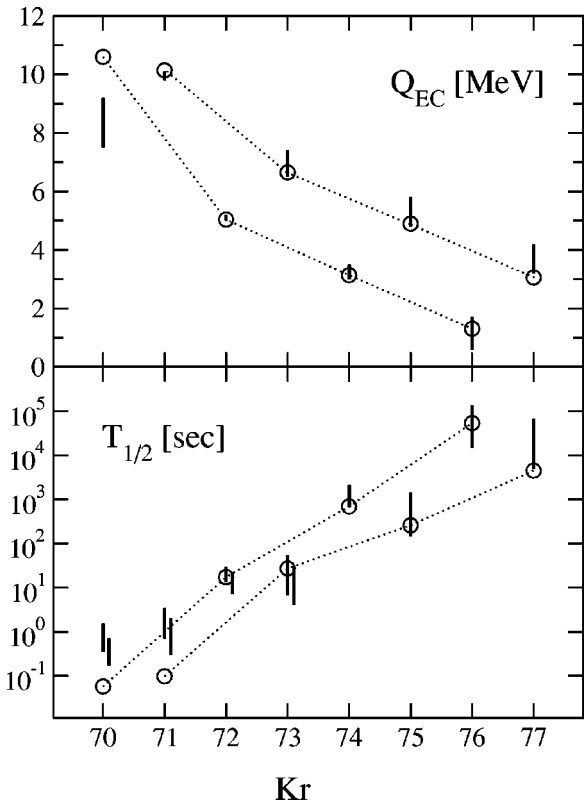

FIG. 16. Experimental Q_{EC} values (top) and half-lives (bottom) for the Kr isotopes are given by circles. The solid vertical lines correspond to our theoretical QRPA calculations. The lengths of the vertical lines indicate the different results we obtain from using the forces SG2 and Sk3 and the possible shapes in each isotope.

IV. CONCLUSIONS AND FINAL REMARKS

We have applied a self-consistent deformed HF+BCS +QRPA formalism with density-dependent effective Skyrme interactions to the description of the β-decay properties of proton-rich odd and even Kr isotopes. This approximation has the appealing feature of treating the excitations and the ground state in a self-consistent framework with basically no free parameters. Our spin-isospin residual interaction contains a particle-hole part, which is derived self-consistently from the Skyrme force, and a particle-particle part, which is a separable force representing a neutron-proton pairing force.

We have analyzed the similarities and differences in the treatment and in the results of even-even and odd-*A* nuclei. The low-lying GT response of odd-*A* nuclei is generated by transitions involving the state of the odd nucleon (1qp transitions). Thus, the excitation spectrum up to twice the pairing gap parameter of neutrons (protons) in the β^+ decay of an odd neutron (proton) parent gives information on the proton (neutron) states. When this low energy strength in the odd-*A* nuclei is removed, the resulting GT strength distribution is very similar to that of the even-even neighbor displaced to higher excitation energy ($E_{ex} \sim 2\Delta$).

In odd-*A* deformed nuclei, for each allowed intrinsic GT transition, one has a set of transitions to rotational states with decreasing strength at higher energies. This is a characteristic of odd-*A* deformed nuclei, which is not present in the spherical limit. The GT strength corresponding to transitions to states in a given band is reduced by geometrical factors involving angular momenta. The energy separation depends on the angular momentum of the transition with a global scale determined by the moment of inertia.

We have found a reasonable agreement with available experimental data. We have also discussed what can be learned from future comparison of our results with experimental data from ISOLDE that are expected very soon. This comparison would be interesting for several reasons: (i) From our study of the dependence on the shape of the GT strength distributions we conclude that information on the shape of the parent nucleus can be gained when data in the whole Q_{EC} window becomes available. We have identified particular narrow regions in the excitation spectra of various nuclei where data could be more conclusive on the nuclear shape. (ii) Comparison to data would be desirable before considering further theoretical refinements, such as the effects of the continuum, the neutron-proton pairing at the mean field level, or extensions of the RPA. (iii) An important point will be to check whether our calculations produce the same level of agreement in all the isotopes or some special characteristics can be found in $N=Z$ nuclei. For the moment, an interesting feature found is the deviation between theory and experiment in the half-life of ^{70}Kr. From the present calculation, this deviation can be attributed to the difference between experimental and theoretical Q_{EC} values, which in turn can be a signature of an extra binding in the $N=Z$ odd-odd daughter nucleus.

ACKNOWLEDGMENTS

We are thankful to M.J.G. Borge, Ch. Miehé, W. Gelletly, and E. Roeckl for stimulating comments and discussions. This work was supported by DGESIC (Spain) under Contract No. PB98-0676.

[1] C. Détraz and D.J. Vieira, Annu. Rev. Nucl. Part. Sci. **39**, 407 (1989); A. Mueller and B.M. Sherrill, *ibid.* **43**, 529 (1993); A.C. Mueller *et al.*, NuPECC report on "Nuclear Structure under Extreme Conditions of Isospin, Mass, Spin and Temperature," 1997.

[2] F.K. Thielemann *et al.*, NuPECC report on "Nuclear and Particle Astrophysics," 1998; M. Arnould and K. Takahashi, Rep. Prog. Phys. **62**, 395 (1999).

[3] H. Schatz, A.A. Aprahamian, J. Görres, M. Wiescher, T. Rauscher, J.F. Rembges, F.K. Thielemann, B. Pfeiffer, P. Möller, K.L. Kratz, H. Herndl, B.A. Brown, and H. Rebel, Phys. Rep. **294**, 167 (1998).

[4] I. Hamamoto, Nucl. Phys. **62**, 49 (1965); J.A. Halbleib and R.A. Sorensen, Nucl. Phys. **A98**, 542 (1967); J. Randrup, *ibid.* **A207**, 209 (1973).

[5] J. Krumlinde and P. Möller, Nucl. Phys. **A417**, 419 (1984).

[6] P. Möller and J. Randrup, Nucl. Phys. **A514**, 1 (1990).
[7] M. Hirsch, A. Staudt, K. Muto, and H.V. Klapdor-Kleingrothaus, Nucl. Phys. **A535**, 62 (1991); K. Muto, E. Bender, and H.V. Klapdor, Z. Phys. A **333**, 125 (1989); H. Homma, E. Bender, M. Hirsch, K. Muto, H.V. Klapdor-Kleingrothaus, and T. Oda, Phys. Rev. C **54**, 2972 (1996).
[8] F. Frisk, I. Hamamoto, and X.Z. Zhang, Phys. Rev. C **52**, 2468 (1995); I. Hamamoto and X.Z. Zhang, Z. Phys. A **353**, 145 (1995).
[9] J. Engel, M. Bender, J. Dobaczewski, W. Nazarewicz, and R. Surnam, Phys. Rev. C **60**, 014302 (1999).
[10] I.N. Borzov, S.A. Fayans, and E.L. Trykov, Nucl. Phys. **A584**, 335 (1995); I.N. Borzov, S.A. Fayans, E. Kromer, and D. Zawischa, Z. Phys. A **355**, 117 (1996).
[11] P. Sarriguren, E. Moya de Guerra, A. Escuderos, and A.C. Carrizo, Nucl. Phys. **A635**, 55 (1998).
[12] P. Sarriguren, E. Moya de Guerra, and A. Escuderos, Nucl. Phys. **A658**, 13 (1999).
[13] P. Sarriguren, E. Moya de Guerra, and A. Escuderos, Nucl. Phys. **A691**, 631 (2001).
[14] H. Flocard, P. Quentin, and D. Vautherin, Phys. Lett. **46B**, 304 (1973); M. Beiner, H. Flocard, N. Van Giai, and P. Quentin, Nucl. Phys. **A238**, 29 (1975); P. Quentin and H. Flocard, Annu. Rev. Nucl. Part. Sci. **28**, 253 (1978); P. Bonche, H. Flocard, P.H. Heenen, S.J. Krieger, and M.S. Weiss, Nucl. Phys. **A443**, 39 (1985).
[15] I. Hamamoto and H. Sagawa, Phys. Rev. C **48**, R960 (1993).
[16] A. Petrovici, K.W. Schmid, and A. Faessler, Nucl. Phys. **A605**, 290 (1996); A. Petrovici, K.W. Schmid, A. Faessler, J.H. Hamilton, and A.V. Ramayya, Prog. Part. Nucl. Phys. **43**, 485 (1999); A. Petrovici, K.W. Schmid, and A. Faessler, Nucl. Phys. **A665**, 333 (2000).
[17] N. Van Giai and H. Sagawa, Phys. Lett. **106B**, 379 (1981).
[18] P. Sarriguren, E. Moya de Guerra, and R. Nojarov, Phys. Rev. C **54**, 690 (1996); Z. Phys. A **357**, 143 (1997).
[19] D. Vautherin and D.M. Brink, Phys. Rev. C **5**, 626 (1972); D. Vautherin, *ibid.* **7**, 296 (1973).
[20] M. Vallières and D.W.L. Sprung, Can. J. Phys. **56**, 1190 (1978).
[21] G. Audi and A.H. Wapstra, Nucl. Phys. **A595**, 409 (1995); G. Audi, O. Bersillon, J. Blachot, and A.H. Wapstra, *ibid.* **A624**, 1 (1997).
[22] D.W.L. Sprung, S.G. Lie, M. Vallierès, and P. Quentin, Nucl. Phys. **A326**, 37 (1979); D.W.L. Sprung, S.G. Lie, and M. Vallierès, *ibid.* **A352**, 19 (1981).
[23] Ch. Miehé, Ph. Dessagne, Ch. Pujol, G. Walter, B. Jonson, M. Lindroos, and The ISOLDE Collaboration, Eur. Phys. J. A **5**, 143 (1999).
[24] H. Flocard, P. Quentin, A.K. Kerman, and D. Vautherin, Nucl. Phys. **A203**, 433 (1973).
[25] G.F. Bertsch and S.F. Tsai, Phys. Rep. **18**, 127 (1975).
[26] J. Engel, P. Vogel, and M.R. Zirnbauer, Phys. Rev. C **37**, 731 (1988); V.A. Kuz'min and V.G. Soloviev, Nucl. Phys. **A486**, 118 (1988); K. Muto and H.V. Klapdor, Phys. Lett. B **201**, 420 (1988).
[27] K. Muto, E. Bender, T. Oda, and H.V. Ilapdor-Kleingrothaus, Z. Phys. A **341**, 407 (1992).
[28] A. Bohr and B. Mottelson, *Nuclear Structure* (Benjamin, New York, 1975).
[29] F. Osterfeld, Rev. Mod. Phys. **64**, 491 (1992); E. Caurier, G. Martinez-Pinedo, A. Poves, and A.P. Zuker, Phys. Rev. C **52**, R1736 (1995).
[30] N.B. Gove and M.J. Martin, Nucl. Data Tables **10**, 205 (1971).
[31] M.J.G. Borge and Ch. Miehé (private communication).
[32] I. Piqueras *et al.*, in *Experimental Nuclear Physics in Europe*, edited by B. Rubio *et al.*, AIP Conf. Proc. No. 495 (AIP, Melville, NY, 1999), p. 77.
[33] H. Schmeing, J.C. Hardy, R.L. Graham, and J.S. Geiger, Nucl. Phys. **A242**, 232 (1975); B. Singh and D.A. Viggars, Nucl. Data Sheets **51**, 225 (1987).
[34] D. Lode, W. Pessara, H. Ohlsson, and E. Roeckl, Z. Phys. **260**, 253 (1973); T. Paradellis, A. Houdayer, and S.K. Mark, Nucl. Phys. **A201**, 113 (1973); B. Singh and D.A. Viggars, Nucl. Data Sheets **42**, 233 (1984).
[35] G. de Angelis *et al.*, Proposal to the ISOLDE Committee, 1998; M.J.G. Borge (private communication).
[36] J. Bea, Ph.D. thesis, Universidad de Valencia, 1995; J. Bea, B. Rubio, A. Gadea, L. Garcia-Raffi, J. Rico, J.L. Taín, M.J.G. Borge, O. Temblad, S. Skoda, J. Eberth, H. Keller, R. Kirchner, and E. Roeckl, ''Detailed study of the ^{75}Kr beta decay properties,'' GSI Scientific Report, 1993, p. 55.
[37] M. Oinonen *et al.*, Phys. Rev. C **56**, 745 (1997); **61**, 035801 (2000).
[38] P. Urkedal and I. Hamamoto, Phys. Rev. C **58**, R1889 (1998).